

EVOLUTION OF TIDALLY TRIGGERED MELTWATER PLUMES BELOW ICE SHELVES

Douglas R. MacAyeal

Department of the Geophysical Sciences, University of Chicago, Chicago, Illinois 60637

Abstract. Theory suggests that tidally induced vertical mixing and tidal rectification may trigger basal melting in two widely separated regions of the sub-ice cavity in the Ross Sea. Vertical separation of two meltwater masses observed off the Ross Ice Shelf by others reaffirms this suggestion and provides geochemical evidence useful for testing models of sub-ice shelf meltwater plume evolution. A simple model of this sort is used here to examine the idealized evolution of two meltwater plumes originating at 1,000-m depth and at 250-m depth. Results indicate that melting along the plume path driven by turbulent entrainment of ambient seawater strongly controls the net vertical penetration of the plume as it flows along the sloping ice shelf base. Entrainment-driven melting along the plume path is possible under present climatic conditions, but at depths greater than approximately 550 m. Such melting may be possible at all depths, however, if climatic change were to warm the ambient water column by approximately 0.6°C.

Introduction

Jacobs et al. [this volume] observe an isotopic and hydrographic distinction between two meltwater masses in the open Ross Sea and, as a result, have proposed a dual circulation regime below the ice shelf. Salinity contrast between these two masses constrains their vertical separation within the ambient water column. This vertical distinction has prompted Jacobs et al. to refer conveniently to the two masses as "Deep Ice Shelf Water" (DISW) and "Shallow Ice Shelf Water" (SISW).

The DISW mass is observed between 350 m and 500 m along the central and western portions of the Ross ice front (See Fig. 6c of Jacobs et al. [this volume]). Judging from the observed distribution of ice shelf draft [Bentley, et al., 1979] (also shown in MacAyeal [1984a]), DISW is likely to be in contact with the ice-shelf base along the remote southeastern region of the sub-ice cavity. The circulation regime proposed by Jacobs et al. [this volume] leading to DISW production must, therefore, embody deep penetration into the sub-ice cavity without direct influence on the basal melting regime of the thin portion of

ice shelf near the ice front. The hydrographic and geochemical composition of DISW measured by Jacobs et al. [this volume] confirms this concept of deep thermohaline circulation in that DISW has the properties expected from a mixture of pure glacial meltwater and High Salinity Shelf Water (HSSW), the predominant water type at the seafloor on the Ross Sea continental shelf.

The SISW mass, in contrast to DISW, is observed at, or just below, the sea surface (see Fig. 6c of Jacobs et al. [this volume]). The ice shelf draft patterns suggest that SISW has been in contact with thin ice near the ice front. Jacobs et al. [this volume] suggest that SISW results predominantly from the influx from the continental slope region of a distinct core of relatively warm water (WMCO) to the central part of the Ross Ice Shelf Barrier.

The numerical tidal simulations discussed in companion papers [MacAyeal, 1984a; MacAyeal, this volume] identify two tidal processes that may generate the two meltwater circulation schemes envisioned by Jacobs et al. [this volume]. The companion study presented in this volume suggests that WMCO influx is driven, in part, by tidal rectification along the ice front. Tidal rectification may thus factor into SISW production. The other companion study [MacAyeal, 1984a] suggests that tidally driven vertical mixing erodes density stratification sufficiently to catalyze basal melting below thick ice shelf in the extreme southeastern part of the sub-ice cavity. Tidally driven mixing may thus factor into DISW production.

As an initial test of the hypothetical link between the simulated tidal processes and the observed meltwaters, the evolution of two idealized meltwater plumes are calculated to see how closely they match the observed meltwater properties. A simple stream tube model [Smith, 1975; Killworth, 1977; Bo Pedersen, 1980; Melling and Lewis, 1982] is adapted here to simulate buoyancy driven flow along the sloping base of an idealized ice shelf. The objective is to determine the depth, salinity and oxygen-isotope depletion at the point where the flow breaks free of the ice shelf base and begins to interleave within the ambient stratified water column. It will be

TABLE 1. Plume Simulations

Run	E _o	K	B	z _c , m	x(z _c), km	S _p (z _c)	θ _f (z _c), °C	c(z _c), ‰	w(z _c), km	h(z _c), m
DISW Analog										
1	0.072	0.025	suppressed	-829	0	35.00	-2.568	-0.064	124	25
2	0.072	0.025	calculated	-212	0	34.63	-2.061	-0.203	410	82
3	0.036	0.025	calculated	-262	0	34.66	-2.161	-0.230	233	47
4	0.018	0.025	calculated	-330	0	34.70	-2.210	-0.258	145	29
a	0.072	0.01	calculated	-816	2996	34.94	-2.541	-0.176	112	22
b	0.072	0.1	calculated	-658	954	34.89	-2.417	-0.240	175	35
SISW Analog										
5	0.072	0.025	suppressed	-54	0	34.53	-1.934	-0.078	120	24
6	0.072	0.025	calculated	-27	0	34.52	-1.912	-0.091	124	25
7	0.036	0.025	calculated	-5	0	34.50	-1.895	-0.141	80	16
8	0.018	0.025	calculated	0	0	34.50	-1.891	-0.219	50	10
c	0.072	0.01	calculated	-119	1405	34.55	-1.985	-0.086	202	40
d	0.072	0.1	calculated	0	270	34.32	-1.880	-0.400	55	11

z_c defined to be level where Δ becomes less than 1.0 × 10⁻⁵.

terminated by the entrainment rate of warm ambient water and by the vertical heat flux through the ice. The equation for B is

$$B = \frac{c_o}{L_o} E w_u (\theta(z) - \theta_f) - \frac{k_i}{L_o \rho} w \frac{(\theta_s - \theta_f)}{H} \quad (14)$$

where θ(z) is the temperature of the entrained water, c_o = 4000 J kg⁻¹ °C⁻¹ is the heat capacity of sea water at 0°C, L_o = 3.35 × 10⁵ J kg⁻¹ is the latent heat of melting, and k_i = 2.4 W m⁻¹ is the conductivity of ice at -12°C. It is important to realize that the basal melting rate given by equation (14) applies only to the area in contact with the plume. Elsewhere, B is assumed zero.

The buoyancy of the meltwater Δ_m is given by

$$\Delta_m = \frac{g}{\rho} (\rho - 1000.0) \text{ if } B > 0$$

$$\Delta = \frac{g}{m} (\rho - 1004.0) \text{ if } B < 0 \quad (15)$$

where ρ is the ambient density, the density of salt-free meltwater is assumed to be 1000 kg m⁻³, and the density of water being frozen as basal ice is assumed to be that corresponding to a salinity of 5.0.

The model equations are solved numerically using an Adams-Moulton predictor/corrector scheme given by Young and Gregory [1972]:

$$G_{n+1} = G_n + \frac{\Delta\lambda}{24} [9 F(G_{n+1}^P) + 19 F(G_n) - 5 F(G_{n-1}) + F(G_{n-2})] \quad (16)$$

where

$$G_{n+1}^P = G_n + \frac{\Delta\lambda}{24} [55F(G_n) - 59F(G_{n-1}) + 37F(G_{n-2}) - 9F(G_{n-3})] \quad (17)$$

G is the solution of

$$\frac{\partial G}{\partial \lambda} = F(G) \quad (18)$$

Δλ is the step-size, and F is a "forcing" function depending on G and other parameters. The first three steps are taken using a Euler forward scheme [Young and Gregory, 1972] to initialize the predictor/corrector sequence.

The model integration is halted when the plume breaks free of the ice-shelf base and begins to interleave within the stratified ambient water column. This criterion is taken to be that point, (y_c, z_c) at which the plume buoyancy Δ is so low that the equations for u and β are no longer valid because inertial terms become comparable to buoyancy terms. This critical plume buoyancy is approximately 10⁻⁴ m s⁻². The results are not sensitive to this choice.

Modeling Strategy

The stream-tube model used here to provide insight into buoyancy-driven flow along the ice shelf base is a highly simplified representation of nature. In addition, the parameters chosen to represent the complex physical processes such as friction and entrainment represent conjectures based on values used in other contexts [e.g., Killworth, 1977; Melling and Lewis, 1982]. Without more detailed observation of the sub-ice regime, modeling studies such as this can at best merely identify logical processes to be examined elsewhere through observation or through more sophisticated modeling techniques.

The objectives of the present modeling exercise must be chosen with the above difficulties in mind. Rather than attempt to tune model parameters to better match observations the objectives here are to explore the range of parameter sensitivity and to identify qualitative rules governing sub-ice plume evolution. Specific tasks to be accomplished here are: (1) to display graphs showing the evolution of S , C , and B as functions of λ , (2) to determine the range of depths at which DISW and SISW analogs break free of the ice shelf and interleave within the ambient water column, and (3) to examine the effects of the earth's rotation. To meet these objectives, numerous simulations were undertaken. A description of these simulations is presented in Table 1. Differences among them fall into four categories: (1) initial conditions, (2) parameter values of E and K , (3) artificial suppression of basal melting, and (4) artificial suppression of earth rotation effects.

Two sets of initial conditions are formulated so that both DISW and SISW may be simulated. For DISW production, tidal mixing in the remote portions of the cavity is assumed to cause an initial $5 \times 10^3 \text{ m}^3 \text{ s}^{-1}$ flux of ambient water (idealized HSSW) to equilibrate with the ice shelf at 1000-m depth. This initial flux and that used for SISW production below are arbitrary and based on the assumption that the plume originates as a small flux which subsequently builds through entrainment. The salinity, buoyancy, oxygen-isotope concentration, and temperature of the initial DISW flux are calculated from conservation equations and have values of 34.79, $2.437 \times 10^{-3} \text{ m}^2 \text{ s}^{-2}$, -0.37 ‰ and -2.76°C , respectively.

For SISW production, tidal rectification near the ice front is assumed to cause an initial $5 \times 10^3 \text{ m}^3 \text{ s}^{-1}$ flux of an idealized WMCO having temperature of -1.0°C and salinity 34.65 to equilibrate with the ice shelf at 250-m depth. The idealized salinity is assigned to WMCO so that it would reside at a depth of 250 m in the idealized water column. In reality, the salinity of WMCO is less than 34.5, but this salinity does not occur at any

level in the model's ambient water column. The initial salinity, buoyancy, oxygen-isotope concentration, and temperature of this equilibrated flux are 34.21, $3.45 \times 10^{-3} \text{ m}^2 \text{ s}^{-2}$, -0.53 ‰ , and -2.08°C , respectively. The DISW plume begins at $y = 0$ and $z = -1000 \text{ m}$, and the SISW plume begins at $y = 750 \text{ km}$ and $z = -250 \text{ m}$. These parameters are consistent with the spatial dimensions and velocity scales observed in the Ross Sea.

The nondimensional entrainment parameter E is inversely proportional to the bulk Richardson number and is given by the formula developed by Bo Pedersen [1980] and by Melling and Lewis [1982]:

$$E = E_0 K / (h \Delta u^{-2}) \quad (19)$$

where $E_0 = 0.072$. This parameterization allows the entrainment rate to go up when the stability of the interface separating the plume from the environment goes down. This interfacial stability is measured by the bulk Richardson number $h \Delta u^{-2}$. To test sensitivity, the model is run using values of E_0 reduced by $1/2$ and by $1/4$.

The nondimensional friction parameter K is varied in order to evaluate model sensitivity. For simulations in which earth rotation is disregarded, $K = 2.5 \times 10^{-3}$. This choice is consistent with the value used previously to parameterize friction in shallow water tidal models [MacAyeal, 1984b], and falls within the range applicable to coastal circulation regimes summarized by Ramming and Kowalik [1980]. For simulations in which earth rotation deflects the stream tube, K is assigned one of two possible values, 10^{-1} or 10^{-2} . The higher values of K used when rotation effects are embraced are consistent with the values used in studies by Killworth [1977] (who used 1.5×10^{-1}) and Melling and Lewis [1982] (who used 1.0×10^{-2}). These high values are motivated in this study, and in those previous, by the desire to reduce the deflection angle β . Without such a reduction (e.g., leaving K at 2.5×10^{-3}) the stream tube does not exit the sub-ice region without extending too far ($\sim 10^6 \text{ km}$) along the ice shelf draft contours. The need for high K to reduce β implies that earth rotation effects are counterbalanced by effects associated with coasts, inverted channels in the base of the ice shelf, or with baroclinic instability (meandering). Such effects are not embraced here.

Two regimes are examined in the present study. In one regime, friction and buoyancy balance, and the Coriolis force is assumed balanced by an unspecified force such as a pressure acting on a coast or on the side of an inverted channel in the base of the ice shelf. Optical leveling surveys show ice shelf surface topography indicative of such channels in the southeastern corner of the

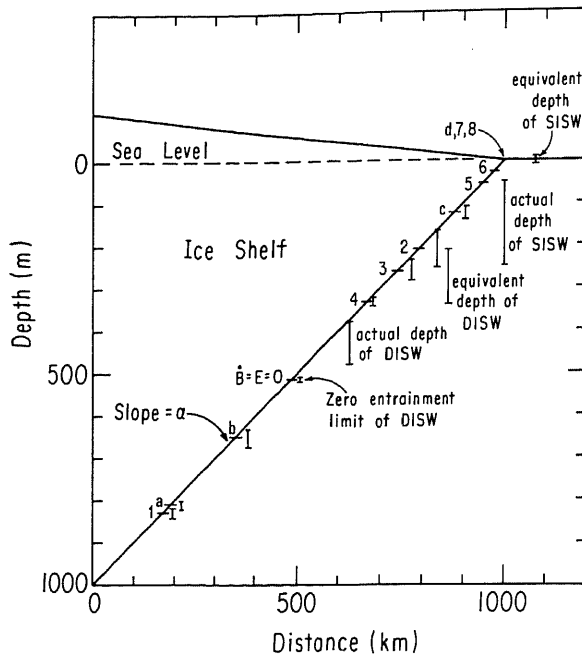


Fig. 2. Levels of plume separation for each model run and the analytic solutions along with the observed depths and equivalent depths of DISW and SISW. The equivalent depth is defined as the depth at which a water mass with its observed temperature and salinity would reside in the idealized ambient water column used in this study. The number and letter identification scheme is summarized in Table 1. In brief, numbered results differ from lettered results by the suppression of earth rotation effects. The results show that rotation effects tend to diminish the vertical penetration of the plume by suppressing entrainment-driven basal melting.

Ross Ice Shelf (near $83^{\circ}58'S$, $160^{\circ}00'W$) [R. Bindschadler, personal communication, 1984]. These channels, however, extend only a limited distance to the north, and are thought to be relict features advected into the ice shelf from grounded ice streams. They may, nevertheless, host meltwater plumes. In this circumstance, β is set to zero, the Richardson number becomes approximately constant at $K/(\sin\alpha \cos\beta)$, and the entrainment parameter E is approximately constant at $E_0 \sin\alpha$.

The other regime represents a geostrophic balance between the Coriolis force and buoyancy. This regime is expected to result in predominantly slow flows in which basal ice topography and coasts exert little influence on the deflection of the stream tube. The Richardson number for this regime is increased by a factor of $\cos^{-1} \beta$ where

$$\beta = \tan^{-1} \left(\frac{fh}{ku} \right)$$

and the entrainment parameter is reduced to approximately 10% of the value derived above for the regime in which buoyancy and friction balance.

Analytic Results

Before discussing the numerical solutions, it is instructive to derive an analytic solution valid for zero entrainment and a quasi-static momentum balance between buoyancy and friction (earth rotation disregarded). The buoyancy and velocity derived from equations (10) and (8) are written as

$$\Delta = \Delta(y = y_0) - N^2 \sin \alpha y \quad (20)$$

and

$$u = \left(h \frac{\sin \alpha}{k} (\Delta(y = y_0) - N^2 \sin \alpha y) \right)^{1/2} \quad (21)$$

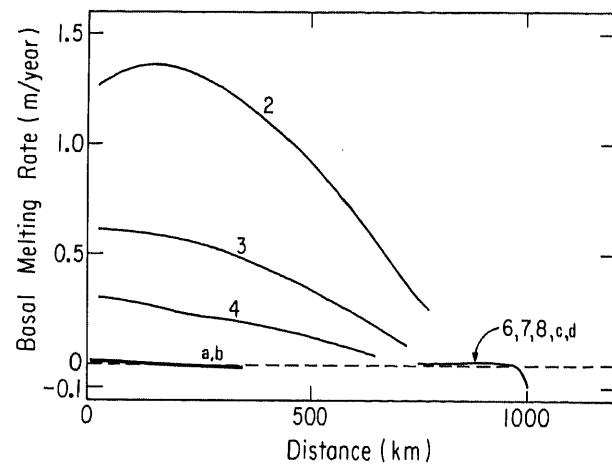


Fig. 3. Melting rates on sections of the ice shelf base with which the plumes are in contact, plotted as functions of y . These ice shelf sections are of the order of 100 km wide. DISW plumes 2, 3, and 4 cause the greatest melting because of their high entrainment rates and the greater temperature difference between the ambient water entrained and the in situ freezing point. These runs demonstrate the effectiveness of entrainment-driven basal melting. The effect of the earth's rotation, however, is to suppress basal melting because the geostrophic balance implies slower flow and less entrainment. The SISW plumes show little basal melting as a result of lower temperature difference between the entrained water and basal ice. High heat flux through the thin idealized ice shelf in contact with the SISW plume also suppresses melting. This suggests that the initial loss of sensible heat from the WMCO dominates near-ice-front melting.

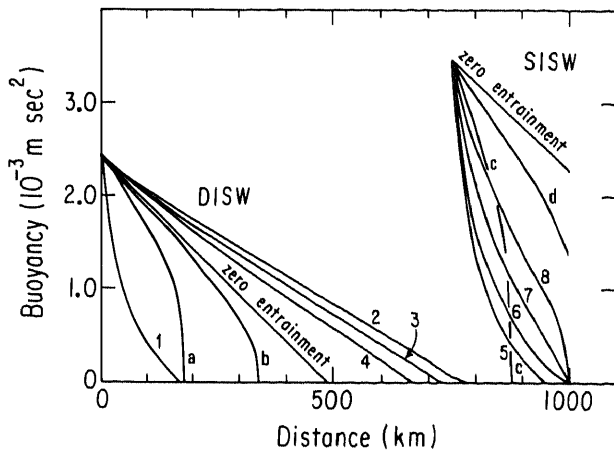


Fig. 4. Plume buoyancy plotted as a function of y . Buoyancy is maintained above the "zero-entrainment" curve for DISW plumes in which earth rotation effects are suppressed. This results from entrainment-driven basal melting. Rotation effects reduce buoyancy below the "zero-entrainment" curve for DISW and SISW plumes. This is because geostrophic balance implies a reduced entrainment rate. Curve a, in which rotation effects buoyancy most strongly, approaches curve 1, which represents the effect of artificial suppression of entrainment-driven basal melting.

where y_0 is the initial value of y or the position of the plume source. From this solution the depths at which the DISW and SISW plume analogs break free of the ice shelf base are

$$z_c = \frac{\Delta(y = y_0)}{N^2} = -516 \text{ (DISW)}$$

$$z_c = 0 \text{ (SISW)} \quad (22)$$

The DISW plume rises along the ice shelf base until it reaches the level where its salinity is equal to the ambient salinity. The SISW plume, in contrast, rises until it reaches the sea surface. This is because the SISW plume has an initial salinity lower than that of the ambient water column at any level. These critical depths are displayed in Figure 2. The velocities along the plume paths are plotted in Figure 3.

Break Free Depths

The numerical results shown in Table 1 and Figure 2 indicate that all the DISW plume analogs interleave within the ambient water column at a considerable depth. No reasonable combination of parameters was found to allow the DISW plume to reach the sea surface. The deepest break free depth (z_c) was attained by run 1 for which rotation and basal melting

were suppressed, and for which the entrainment had its greatest value. The shallowest break free depth was attained by run 2 for which rotation, but not basal melting, was suppressed. Runs 2 through 4 indicate that increasing entrainment reduces the break free depth. This relationship occurs because greater entrainment incorporates more heat into the plume which subsequently produces more meltwater. Figures 3 and 4 show the basal melting rate (B) and plume buoyancy (Δ), as functions of y , respectively. Entrainment-driven melting is demonstrated by these figures to reduce DISW buoyancy decay, therefore allowing greater vertical penetration.

The effect of earth rotation on the DISW plume is to deepen the break free depth below the zero-entrainment limit determined analytically and shown in Figure 2. As seen in Figure 5, the geostrophic balance of runs a and b (letters denote runs with rotation effects) suppresses the plume velocities. This suppression tends to reduce the entrainment rate which subsequently reduces the basal melting rate (Figure 3). The buoyancy decay with increasing y tends to fall below the zero-entrainment limit, however, because the plume path is not directly along the y axis.

In comparing the break free depth predicted by the model with the observed depth of DISW along the ice front [Jacobs, et al., this volume] it is useful to define an "equivalent observed depth." This definition allows the observed depth to be corrected for the fact that the salinity (density) stratification of the

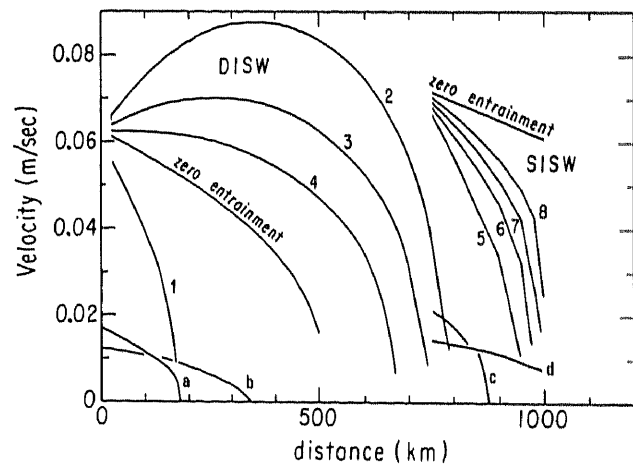


Fig. 5. The plume velocities are plotted as functions of y . Numbered plumes (earth rotation suppressed) accelerate rapidly downstream of their sources to reach a velocity characterized by balance between friction and buoyancy. Lettered plumes move more slowly as is characterized by the geostrophic balance. Velocity maxima associated with plumes 2 and 3 are caused by the effect of plume thickness.

natural water column is not uniform. The observed salinity of DISW is between 34.63 and 34.73; thus if the actual DISW mass were to reside in the idealized sea, it would occupy the depth range between 217 m and 383 m. This falls precisely within the range of break free depths spanned by the DISW plume experiments in which earth rotation effects are ignored. Possible implications of this comparison are: (1) the natural DISW plume is channeled by a coastline, by the ice-shelf topography or by horizontally nonuniform stratification; (2) the natural DISW plume originates much higher in the water column, closer to the depth at which it interleaves within the open ocean.

In contrast with the simulated DISW plume, the simulated SISW plume generally emerges at the sea surface unless entrainment is enhanced by a high value of the entrainment parameter and by suppression of earth rotation effects. Also unlike the DISW plume, sensible heat entrained into the SISW plume is negligible because shallow depth implies that the ambient water column temperature is close to the basal ice temperature. Without entrainment-driven melting along the plume path (Figure 3), entrainment simply forces a more rapid plume buoyancy decay (Figure 4).

The equivalent depth for SISW is sea level in the idealized sea rather than at depth [Jacobs et al., this volume]; thus the tendency for the modeled SISW plume to reach the sea surface before breaking free of the ice is consistent with observation. This agreement may be fortuitous, however, because the substantial idealizations of WMCO influx and ambient temperature may emphasize incorrect natural processes. The SISW experiments demonstrate that basal melting near the ice front is not likely to be sustained by entrained sensible heat from HSSW. The results here confirm that sensible heat flux associated with inflowing WMCO and with seasonal upper-ocean warming is the dominant factor for near-ice-front melting.

Entrainment-Driven Melting

The numerical simulations may be organized into two categories besides those of DISW and SISW production depending on whether the entrainment helps or hinders the maintenance of plume buoyancy. All the SISW simulations, and the DISW simulations in which rotation effects are embraced, show that entrainment increases the buoyancy decay rate above the "zero-entrainment limit" determined analytically (Figure 4). The DISW plume simulations represented by runs 1, 2, and 3 display the opposite effect as a result of entrainment-driven melting. This result suggests that a critical depth exists below which entrainment-driven melting is able to counterbalance the otherwise buoyancy reducing effects of entrainment.

To estimate this critical depth, equation (10) is simplified by assuming that the change of buoyancy flux with λ is mostly due to changing buoyancy rather than changing volume flux

$$\left(\Delta \frac{\partial(Au)}{\partial \lambda} \ll Au \frac{\partial \Delta}{\partial \lambda} \right) :$$

$$\frac{\partial \Delta}{\partial \lambda} = \frac{1}{Au} \{ \dot{B} \Delta_m - (Ewu)\Delta \} - N^2 \sin \alpha \cos \beta \quad (23)$$

The last term on the right hand side of equation (23) expresses the zero-entrainment limit of buoyancy decay that depends entirely on the vertical motion of the plume with respect to the density stratified environment. Depending on whether the first term on the right hand side of equation (23) is positive or negative, entrainment will either diminish or enhance plume buoyancy decay. If the basal melting rate given by equation (14) is substituted into equation (23) and the vertical heat flux through the ice is disregarded, the difference $\theta(z) - \theta_f$ determines whether $(\dot{B}\Delta_m - (Ewu)\Delta)$ is positive or negative. The criterion for whether entrainment helps or hinders buoyancy decay is thus

$$\theta(z) - \theta_f > \frac{\Delta}{\Delta_m} \frac{L_o}{C_o} \quad (24)$$

This criterion can be simplified and expressed in terms of depth by assuming $\theta(z) \cong 1.87^\circ\text{C}$, using a representative value $\Delta/\Delta_m \cong 5 \times 10^{-3}$, and by adopting in place of equation (1)

$$\theta_f \cong -1.87 + 7.59 \times 10^{-3} m^{-1} z \quad (25)$$

This alternative criterion is roughly

$$z < -550 \text{ m} \quad (26)$$

where the value 550 m may be changed depending on the value chosen to represent the ratio Δ/Δ_m .

The implication of this criterion is that only DISW plumes are susceptible to buoyancy enhancement by entrainment-driven melting. The SISW plumes flow through an environment where sensible heat entrainment and melting is too low to counterbalance the additional density attained when plume and environment mix. If climatic change were to warm the ambient temperatures above approximately -1.3°C , the criterion expressed by equation (24) would be met at all depths. SISW plumes would thus induce entrainment-driven melting, and would become more prominent in their effect on the ice shelf mass balance.

Evolution of Plume Geochemistry

Jacobs et al. [this volume] associate meltwaters observed in the open Ross Sea with parent water masses by examining the effects of

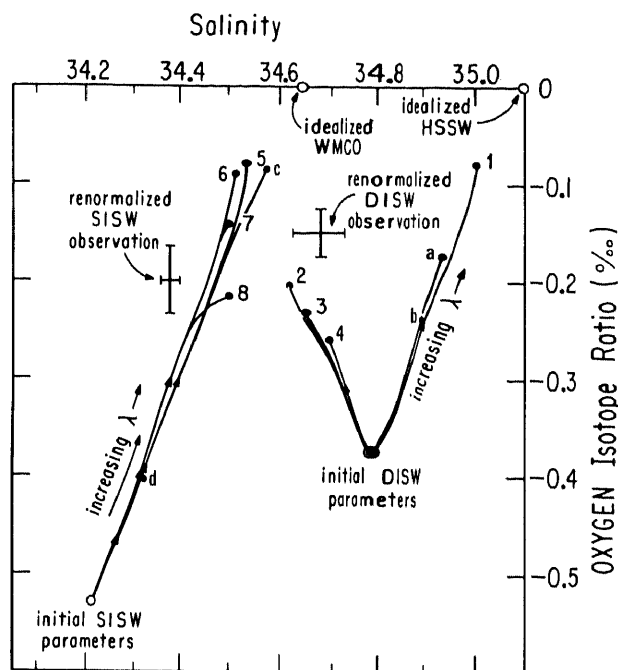


Fig. 6. Plume evolutions expressed as parametric curves in S_p versus c space. Without rotational effects, the DISW plumes reduce their salinity as their oxygen-isotope concentrations increase (become less negative) because entrainment tends to elicit further melting. SISW plumes and DISW plumes effected by earth rotation evolve in the opposite sense because, without strong melting, entrainment always increases their salinity. End points of the parametric curves are compared with the observed S_p and c of DISW and SISW normalized to account for the adjusted S_p and c values assigned to HSSW and WMCO. This renormalization of the observations is required to account for the assumption that the ambient water column has a constant vertical salinity gradient. Without this renormalization the model results and data cannot be directly compared. Best agreement with "observation" is attained for SISW runs with moderate entrainment.

melting on the salinity and oxygen-isotope composition. The diagram of salinity versus oxygen-isotope ratio of the plume shown in Figure 6 indicates the simulated geochemical evolution of the two meltwater masses as they travel from their respective points of origin to where they interleave into the open ocean. For both DISW and SISW plumes, the oxygen-isotope ratios are expressed relative to the initial ratios of the respective WMCO and HSSW input water masses. These input water masses are assumed to have an oxygen-isotope ratio of 0 ‰ rather than the slightly negative values given by Jacobs et al. [this volume]. This renormalization, or recalibration, must

be accounted for when comparing Figure 6 with its counterpart in Jacobs et al. [this volume].

For DISW, best agreement between the simulated plume properties at the break free depth and the renormalized observation is for the run having largest entrainment-driven basal melting (run 2). By suppressing this form of melting, earth rotation effects tend to increase the plume salinity along the plume path. Otherwise, meltwater dilution causes the plume salinity to decrease along the plume path.

Entrainment-driven melting is negligible for the simulated SISW plumes; thus plume salinity increases along the plume path for all runs. Best agreement between simulation and renormalized observation is achieved for runs in which entrainment is suppressed by earth rotation or by a small value of the entrainment parameter.

Ice Shelf Mass Balance

The entrainment-sustained basal melting described above has several serious drawbacks which presumably can be corrected in a more realistic study. The most apparent defect is that basal melting is probably too high for the DISW plume and probably too low for the SISW plume. This judgment is based on the tentative perception of the overall mass budget of the Ross Ice Shelf presented by MacAyeal and Thomas [1984]. Modeled and observed ice shelf flow patterns suggest that two areas of melting are required to maintain a steady state ice thickness distribution on the Ross Ice Shelf. These areas are: (1) between the Cray Ice Rise and Siple Coast, and (2) within 100 km of the ice front (especially near the location of the warm core). The modeled DISW plumes, in contrast, elicit a basal melting pattern that persists along the entire plume trajectory. Furthermore, the modeled SISW plumes produce appreciable melting only at their points of origin.

This apparent model defect may, in future studies, be corrected by: (1) allowing feedback between the basal melting rates and the internal ice shelf temperatures, (2) adjusting the temperature and salinity stratification of the ambient seawater to conform with the observed hydrography, and (3) allowing the plume to determine, in concert with other factors, the stratification of the ambient water column. The first correction would intensify the vertical heat flux at the ice-ocean contact and halt or diminish basal melting downstream of the plume origin [MacAyeal, 1979]. This effect could account for the apparent lack of melting associated with the possible DISW plume in the central part of the Ross Sea cavity. The second correction would allow greater basal melting along the ice front,

where ambient water in summer [Pillsbury and Jacobs, this volume] has a temperature of -1.25°C , or warmer, rather than the colder temperature assumed in the model. The third correction would diminish basal melting associated with the DISW plume because recirculation of meltwater back into the sub-ice cavity would diminish the heat available to be entrained. Additional factors to be addressed in an improved study of meltwater plume evolution are: instabilities, coastal boundary effects, variable ice shelf thickness gradients, variable ice shelf oxygen-isotope concentration, and time-dependent ambient stratification.

Conclusion

Buoyant meltwater plumes flowing along the base of large Antarctic ice shelves interleave within the surrounding ocean at depths determined by the ice shelf draft at the plume source and the degree of entrainment experienced along the plume trajectory. Model studies presented here suggest that DISW plumes, or plumes originating where the ice shelf draft is greater than approximately 500 m, tend to penetrate vertically farther than do SISW plumes. This result is a consequence of basal ice shelf melting forced by the sensible heat flux accompanying plume entrainment. The geostrophic balance tends to mitigate this effect because plume velocity and entrainment rates are reduced when the Coriolis force, rather than friction, balances the buoyancy force.

The capacity for ventilating a typical sub-ice shelf cavity is strongest for the most vigorous DISW plumes in which rotation effects are suppressed and entrainment parameters are set high. Assuming a return flow of HSSW, the outgoing DISW plume represented by run 2 (Table 1), for example, would flush the entire cavity below the Ross Ice Shelf in approximately 2 years. If averaged over the entire ice shelf area, the ablation rate driven by plume entrainment would be approximately 0.2 m/yr.

Such vigorous sub-ice shelf flushing by a DISW plume is not anticipated in the Ross Sea, however, because earth rotation effects are likely to suppress necessary entrainment-driven melting. The rotational effects referred to here would be cancelled by the presence of coast or inverted "channels" in the ice-shelf base. That may explain the relatively vigorous flushing observed by Potter and Paren [this volume] below the George VI Ice Shelf. Comparison between the simulated evolution of plume geochemistry and the hydrographic properties of DISW observed by Jacobs et al. [this volume] suggests that the real DISW plume may originate where the Ross Ice Shelf has a draft of approximately 600 m

rather than 1000 m as was assumed in this study. Some areas in the southeastern corner of the ice shelf (near $87^{\circ}37'S$, $166^{\circ}00'W$) have an ice thickness of approximately 600 m and additionally display ice flow convergence requiring greater than 0.5 m/yr melting to maintain steady state [R. Bindshadler, personal communication, 1984].

In contrast to the DISW plumes, SISW plumes caused by WMCO impingement on an ice shelf base at 250 m depth do not have the capacity for entrainment-driven melting. As a result, the geochemical evolution of SISW represents a simple mixture of plume with ambient water. The net basal ablation associated with SISW production is, furthermore, entirely associated with the plume source where sensible heat from the WMCO is lost. Entrainment-driven basal melting similar to that associated with possible DISW plumes could be sustained, however, if the ambient water through which the SISW plume flows had a temperature greater than approximately -1.3°C . Temperatures this warm near the surface of the Ross Sea are not characteristic of the present climatic regime; but could be expected if CO_2 warming were to occur.

Acknowledgments. I sincerely appreciate the scientific advice and editorial assistance of S. Jacobs, several anonymous reviewers, and G. York. This work was supported by a grant from the National Science Foundation (DPP 84-01016).

References

- Bentley, C. R., J. W. Clough, K. C. Jezek, and S. Shabtaie, Ice-thickness patterns and the dynamics of the Ross Ice Shelf, Antarctica, *J. Glaciol.*, 24(90), 287-294, 1979.
- Bo Pedersen, F., Dense bottom currents in a rotating ocean, *J. Hydraul. Div. Am. Soc. Civ. Eng.*, 106(HY8), 1291-1308, 1980.
- Fujino, K., E. L. Lewis, and R. G. Perkin, The freezing point of seawater at pressures up to 100 bars, *J. Geophys. Res.*, 79(12), 1792-1797, 1974.
- Gill, A.E., Circulation and bottom water production in the Weddell Sea, *Deep Sea Res.*, 20, 111-140, 1973.
- Gill, A.E., *Atmosphere-Ocean Dynamics*, 662 pp., Academic Press, New York, 1982.
- Grootes, P.M., and M. Stuiver, Ross Ice Shelf and Dome C oxygen-isotope analysis, *Antarct. J. U.S.*, 17(5), 76-78, 1982.
- Jacobs, S.S., A.L. Gordon, and J.L. Ardai, Jr., Circulation and melting beneath the Ross Ice Shelf, *Science*, 203(4379), 441-443, 1979.
- Jacobs, S.S., R.G. Fairbanks, and Y. Horibe, Origin and evolution of water masses near the Antarctic continental margin: Evidence from $\text{H}_2^{18}\text{O}/\text{H}_2^{16}\text{O}$ ratios in seawater, this volume.

- Killworth, P.D., Mixing on the Weddell Sea continental slope, Deep Sea Res., 24, 427-448, 1977.
- MacAyeal, D.R., Transient Temperature-Depth Profiles of the Ross Ice Shelf, M.Sc. thesis, 116 pp., Univ. of Maine at Orono, May 1979.
- MacAyeal, D.R., Thermohaline circulation below the Ross Ice Shelf: A consequence of tidally induced vertical mixing and basal melting, J. Geophys. Res., 89(C1), 597-606, 1984a.
- MacAyeal, D.R., Numerical simulations of the Ross Sea tides, J. Geophys. Res., 89(C1), 607-615, 1984b.
- MacAyeal, D.R., Tidal rectification below the Ross Ice Shelf, Antarctica, this volume.
- MacAyeal, D.R., and R. H. Thomas, The effects of basal melting on the present flow of the Ross Ice Shelf, J. Glaciol., in press, 1984.
- Melling, H., and E.L. Lewis, Shelf drainage flows in the Beaufort Sea and their effect on the Arctic Ocean pycnocline, Deep Sea Res., 29(8A), 967-985, 1982.
- Millero, F.J., Freezing point of sea water, Eighth Report of the Joint Panel of Oceanographic Tables and Standards, Appendix 6, UNESCO Tech. Pap. Mar. Sci., 28, 29-35, Pillsbury, R.D. and S.S. Jacobs, Preliminary observations from long-term current meter moorings near the Ross Ice Shelf, Antarctica, this volume.
- Potter, J.R., and J.G. Paren, Interaction between ice shelf and ocean in George VI Sound, Antarctica, this volume.
- Ramming, H.G., and Z. Kowalik, Numerical Modeling of Marine Hydrodynamics, Applications to Dynamic Physical Processes, Elsevier Oceanography Series No. 26, Elsevier/North Holland, New York, 368 pp., 1980.
- Smith, P.C., A stream-tube model for bottom boundary currents in the ocean, Deep Sea Res., 22, 853-873, 1975.
- Thomas, H.G., D.R. MacAyeal, D.H. Eilers, and D.R. Gaylord, Glaciological studies on the Ross Ice Shelf, Antarctica, 1973-1978, in The Ross Ice Shelf: Glaciology and Geophysics, Ant. Res. Ser., vol. 40, edited by C.R. Bentley and D.E. Hayes, pp. 21-53, American Geophysical Union, Washington, D.C., 1984.
- Young, D.M., and R. T. Gregory, A Survey of Numerical Mathematics, vol. 1, 492 pp., Addison-Wesley, Reading, Pa., 1972.

(Received October 18, 1984;
accepted December 27, 1984.)